Progress on the New Generation of Chinese Meteorological Satellites and Some Applications

DONG Chaohua*, ZHANG Wenjian

National Satellite Meteorological Center of CMA,
46, Zhong GuanCun Nan Dajie, Beijing 100081, CHINA

Abstract

This paper concentrates on the recent research progress, such as the applications in dust storm, cloud thermodynamic phase analysis and numerical weather prediction, as well as the new generation of Chinese meteorological satellite programs.

Keyword: Meteorological satellite, new generation, dust storm, radiance

1. Introduction

The National Satellite Meteorological Center (NSMC) was established within the Chinese Meteorological Administration (CMA) in 1970. The responsibility of NSMC is to operate, manage, and improve the Nation's operational meteorological satellite system; to make requirements for new satellites; to archive and disseminate satellite data/ products to meet the need of users in public, decision making, private, and scientific research programs.

China has Launched six meteorological satellites, four of them are sun-synchronous, two of them are geostationary satellites, and will continue its two types of meteorological satellite programs. Characteristics of the Chinese new generation payload for polar orbit are described specifically in this paper. The new generation for Chinese geostationary Meteorological satellite is only in a proposal stage. This paper just briefly introduces the current progress on meteorological satellite application research and new generation of Chinese Meteorological satellite programs.

2. New Generation of Chinese Meteorological Satellites

2.1 Polar orbiting meteorological satellite

FY-3 series, the second generation of Chinese polar orbiting meteorological satellites is now under construction. The first satellite will be launched in 2006. The main mission objectives of FY-3 are:

- To provide global sounding of 3-dimensional atmospheric thermal and moisture structures, cloud and precipitation parameters to support global numerical weather prediction.
- To provide global images to monitor large scale meteorological and/or hydrological disasters and biosphere environment anomalies.
- To provide important geophysical parameters to support study on global change and climate prediction.
- To perform data collection.

To achieve the above objectives, the FY-3 system satellites will have a meteorological and

* Dchua@nsmc.cma.gov.cn; Phone (86-10)68406237; fax (86-10)62172724

environmental payload as follows:

- The Imaging Mission:
  - VIRR Visible and InfRared Radiometer
  - MERSI Medium Resolution Spectral Imager
  - MWRI Microwave Radiation Imager

- The Sounding Mission
  - IRAS InfraRed Atmospheric Sounder
  - ASI Atmospheric Sounding Interferometer
  - MWTS MicroWave Temperature Sounder
  - MWHS MicroWave Humidity Sounder
  - SBUV Solar Backscatter Ultraviolet Sounder
  - TOU Total Ozone Unit

- The Complementary Mission
  - SIM Solar Irradiation Monitor
  - ERM Earth Radiation Measurement
  - SEM Space Environment Monitor

FY-3 will have a sun-synchronous orbit at 836km, crossing the Equator in a southward direction at 1010 Local time. The spacecraft will weigh a total of 2200kg.The number of channels, scan spots and spatial resolution for each instrument are listed in Table 2.1.

Table 2.1 Basic Information for each Instrument

Name of Instrument	Number of Channels	Field of Views /line	Spatial Resolution at Sub point
VIRR	10	2048	1.1
IRAS	26	56	17
MWTS	4	15	50/75
MWHS	5	90	15
MERSI	20	2048/8192	1.1/250
SBUS	12	240	70/10
TOU	6	31	50
MWRI	6	240	15-70
ASI	TBD		

The characteristics of VIRR, IRAS, WWTS, WMHS, MERSI, SBUS, TOU are shown in Tables 2.2-2.9, respectively.

Table 2.2 Visible and Infrared Radionmeter (VIRR) Channel Characteristics

Channel No.	Wavelength (μm)	Dynamic range	Detecting Sensitivity
1	0.58~0.68	ρ : 0~90%	S/N≥3(ρ =0.5%)
2	0.84~0.89	ρ : 0~90%	S/N≥3(ρ =0.5%)
3	3.55~3.95	190~340K	NE Δ T≤0.4K(300K)
4	10.3~11.3	190~330K	NE Δ T≤0.22K(300K)
5	11.5~12.5	190~330K	NE Δ T≤0.22K(300K)
6	1.58~1.64	ρ :0~80%	S/N≥3(ρ =0.5%)
7	0.43~0.48	ρ :0~50%	S/N≥3(ρ =0.5%)
8	0.48~0.53	ρ :0~50%	S/N≥3(ρ =0.5%)
9	0.53~0.58	ρ :0~50%	S/N≥3(ρ =0.5%)
10	0.900~0.965	ρ :0~90%	S/N≥3(ρ =0.5%)

Table 2.3 IRAS Channel Characteristics

Channel No.	Channel Central		Half-Power Band Width (cm^{-1})	Main Absorber	Max.Scene Temperature (K)	NE△N (mW/m^2-sr-cm^{-1})
	(ch^{-1})	(μm)				
1	669	14.95	3	CO_2	280	4.00
2	680	14.75	10	CO_2	265	0.80
3	690	14.49	12	CO_2	250	0.60
4	703	14.22	16	CO_2	260	0.35
5	716	13.97	16	CO_2	275	0.32
6	733	13.84	16	CO_2/H_2O	290	0.36
7	749	13.35	16	CO_2/H_2O	300	0.30
8	802	12.47	30	Window	330	0.20
9	900	11.11	35	Window	330	0.15
10	1030	9.71	25	O_3	280	0.20
11	1345	7.43	50	H_2O	330	0.23
12	1365	7.33	40	H_2O	285	0.30
13	1533	6.52	55	H_2O	275	0.30
14	2188	4.57	23	N_2O	310	0.009
15	2210	4.52	23	N_2O	290	0.004
16	2235	4.47	23	CO_2/N_2O	280	0.006
17	2245	4.45	23	CO_2/N_2O	266	0.006
18	2388	4.19	25	CO_2	320	0.003
19	2515	3.98	35	Window	340	0.003
20	2660	3.76	100	Window	340	0.002
21	14500	0.69	1000	Window	100%A	0.10%A
22	11299	0.885	385	Window	100%A	0.10%A
23	10638	0.94	550	H_2O	100%A	0.10%A
24	10638	0.94	200	H_2O	100%A	0.10%A
25	8065	1.24	650	H_2O	100%A	0.10%A
26	6098	1.64	450	H_2O	100%A	0.10%A

Table 2.4 MWTS Channel Characteristics

Channel No.	Central Frequency (CHz)	Main Absorber	Band Width (MHz)	NE△T (k)	Antenna Beam Efficiency (%)	Dynamic Range (K)
1	50.30	Window	180	0.5	>90	3-340
2	53.596±0.115	O_2	2X170	0.4	>90	3-340
3	54.94	O_2	400	0.4	>90	3-340
4	57.290344	O_2	330	0.4	>90	3-340

Table 2.5 MWHS Channel Characteristics

Channel No.	Central Frequency (CHz)	Main Absorber	Band Width (MHz)	NE△T (k)	Antenna Beam Efficiency (%)	Dynamic Range (K)
1	150(V)	Window	2000	0.9	≥95%	3-340
2	150(H)	Window	2000	0.9	≥95%	3-340
3	183.31±1	H2O	500	1.1	≥95%	3-340
4	183.31±3	H2O	1000	0.9	≥95%	3-340
5	183.31±7	H2O	2000	0.9	≥95%	3-340

Table 2.6 Moderate Medium Spectral Imager (MERSI)
Channel Characteristics

Channel No.	Central Wavelength (μm)	Band Width (μm)	Sub-point Resolution (m)	NEΔT ρ (%) K (300K)	Dynamic Range(ρ),(K)
1	0.470	0.05	250	0.45	100%
2	0.550	0.05	250	0.4	100%
3	0.650	0.05	250	0.3	100%
4	0.865	0.05	250	0.3	100%
5	11.25	2.5	250	0.4K	330K
6	0.412	0.02	1000	0.1	80%
7	0.443	0.02	1000	0.1	80%
8	0.490	0.02	1000	0.05	80%
9	0.520	0.02	1000	0.05	80%
10	0.565	0.02	1000	0.05	80%
11	0.650	0.02	1000	0.05	80%
12	0.685	0.02	1000	0.05	80%
13	0.765	0.02	1000	0.05	80%
14	0.865	0.02	1000	0.05	80%
15	0.905	0.02	1000	0.10	90%
16	0.940	0.02	1000	0.10	90%
17	0.980	0.02	1000	0.10	90%
18	1.030	0.02	1000	0.10	90%
19	1.640	0.05	1000	0.05	90%
20	2.130	0.05	1000	0.05	90%

Table 2.7 Solar Backscatter Ultraviolet Sounder(SBUS)
Channel Characteristics

Channel No.	Central Wavelength (nm)	Band Width (nm)
1	252.00±0.05	1+0.2, -0
2	273.62±0.05	1+0.2, -0
3	283.10±0.05	1+0.2, -0
4	287.70±0.05	1+0.2, -0
5	292.29±0.05	1+0.2, -0
6	297.59±0.05	1+0.2, -0
7	301.97±0.05	1+0.2, -0
8	305.87±0.05	1+0.2, -0
9	312.57±0.05	1+0.2, -0
10	317.56±0.05	1+0.2, -0
11	331.26±0.05	1+0.2, -0
12	339.89±0.05	1+0.2, -0
Cloud Cover Radiometer	379.00±1.00	3+0.3

Table 2.8 Total Ozone Unit (TOU)
Channel Spectrum Characteristics

Channel No.	Central Wavelength (nm)	Band Width (nm)
1	308.68±0.15	1+0.3, -0
2	312.59±0.15	1+0.3, -0
3	317.61±0.15	1+0.3, -0
4	322.40±0.15	1+0.3, -0
5	331.31±0.15	1+0.3, -0
6	360.11±0.25	1+0.3, -0

Table 2.9 Microwave Radiation Imager (MWRI) Channel Spectrum Characteristics

Channel No.	Central Frequency (GHz) Polarization		Main Absorber	Band Width (MHz)	NE△T (K)	Antenna Beam Efficiency	Dynamic Range (K)
1	10.65	V.H	Window	180	0.5	≥90%	3-340
2	18.7	V.H	Window	200	0.5	≥90%	3-340
3	23.8	V.H	H2O	400	0.8	≥90%	3-340
4	36.5	V.H	Window	900	0.5	≥90%	3-340
5	89	V.H	Window	4600	1.0	≥90%	3-340
6	150	V.H	Window	3000	1.3	≥90%	3-340

2.2 Geostationary meteorological satellites

Geostationary meteorological satellite FY-4 series, the second generation of Chinese geostationary meteorological satellites is now in the concept design phase. Considerations for the FY-4 system are as follows:

- Three-Axis stabilization
- More powerful imager
- Sounding capability
- Lightning detection
- Data collection
- Powerful ground control capability
- Application and services system

FY-4 is expected to be launched beyond 2010.

3. Progress on Satellite Applications

3.1 Real time monitor and quantitative prediction of Northeast Asian dust storms

From spring to early summer, dust storms frequently occur in Northeast Asian (in some places throughout the year). Northern China was seriously affected by a dust storm and dust weather system in spring. These dust storms and dust weather systems are generally generated in the drought and part drought areas at middle latitudes, which just have a sparse vegetation coverage, as strong winds entrain large quantities of dust particles into the atmosphere and carry them over large distances downstream. These dust storms have a severe impact upon the air quality in regions downwind of the dust sources. The real-time monitoring and prediction of dust storms therefore are highly desirable as a meteorological service to the public.

The payload of meteorological satellites has several spectral regions located at visible, near infrared, infrared and microwave bands so the satellite sensors can receive reflection, emission and absorption from the observed targets, such as aerosol, clouds, and earth's surface. Based on different spectral signatures, the geophysical parameters can be obtained.

As the meteorological satellites have a wide monitoring scale, good time frequency and spatial resolution and high precision, it is the most effective way for monitoring dust storms (Zheng et al., 2002). A 24 hour operational dust storm monitoring system by using both geostationary and polar orbiting satellite data was established in NSMC/CMA on March 1, 2001. With this system, we can dynamically monitor dust storms, analyze dust storm sources and transport paths, as well as calculate dust storm range of influence and aerosol strength.

A detailed analysis has been done on the influence of dust storms reaching Beijing. We find that there are two major sources of dust storm, one is in Mongolia, the other is in the Inner Mongolia Autonomous Region and northern part of Hebei province in 2002. Affected by the Mongolian cyclone and cold front systems in spring, the dust storm occurred in Mongolia and continuously strengthened on the way, it would affect a wide area and had a high strength.

The dust storm influencing Beijing has three paths based on the meteorological satellite observations, during the spring time of 2002. A. from Mongolia to Beijing via Hunsandake Desert in the Inner Mongolia Autonomous Region and Hei-he in Hebei province; B. from Zhurihe to Beijing via Zhangjiakou in Hebei province; C. from north Shanxi province to Beijing via Shanggan-he in Hebei province.

The form of dust storm is a very complicated physical process, such as atmospheric movement, type of land surface, dust emission etc. The prediction model of dust activities must involve the key processes of dust emission, dust transport and dust deposition. It requires the coupling of the dust emission scheme with an atmospheric model, supported by other modules and adequate land-surface parameter, i.e., the establishment of an integrated modeling system. The theory and model framework can be found in several publications (Shao 2001; Shao et al., 2002).

In order to test the integrated modeling system, a joint working group in which the scientists are from different institutes, such as the CMA, the Chinese Academy of Science and City University of Hong Kong, China, did 24, 48 and 72hr forecasts of Northeast Asian dust events for March and April, 2002. The results are validated with synoptic records from the meteorological network and dust concentration measurements at 12 stations in China, Japan and Korea. The predicted spatial patterns and temporal evolution of dust events and the predicted near-surface dust concentrations are found to agree well with the observations (see Figure 3.1). In Figure 3.2, successive forecasts of near surface dust concentration for the 10-day period between 15 and 24 March 2002 are compared with observations. The figure demonstrates that the modeling system well predicted the spatial distributions and temporal evolutions of all dust events in this period of time (Shao et al., 2003).

We have determined the total dust emission, total dust deposition and total dust load for the

entire domain of simulation and have found that the total dust emission is on average 11.5 $x10^6$ tn day^{-1} (maximum 65.7 $x10^6$ tn day^{-1}); total dust deposition is 10.8 $x10^6$ tn day^{-1} ((maximum 51.4 $x10^6$ tn day^{-1}) and total dust load is 5.5 $x10^6$ tn with a maximum of 15.9 $x10^6$ tn.

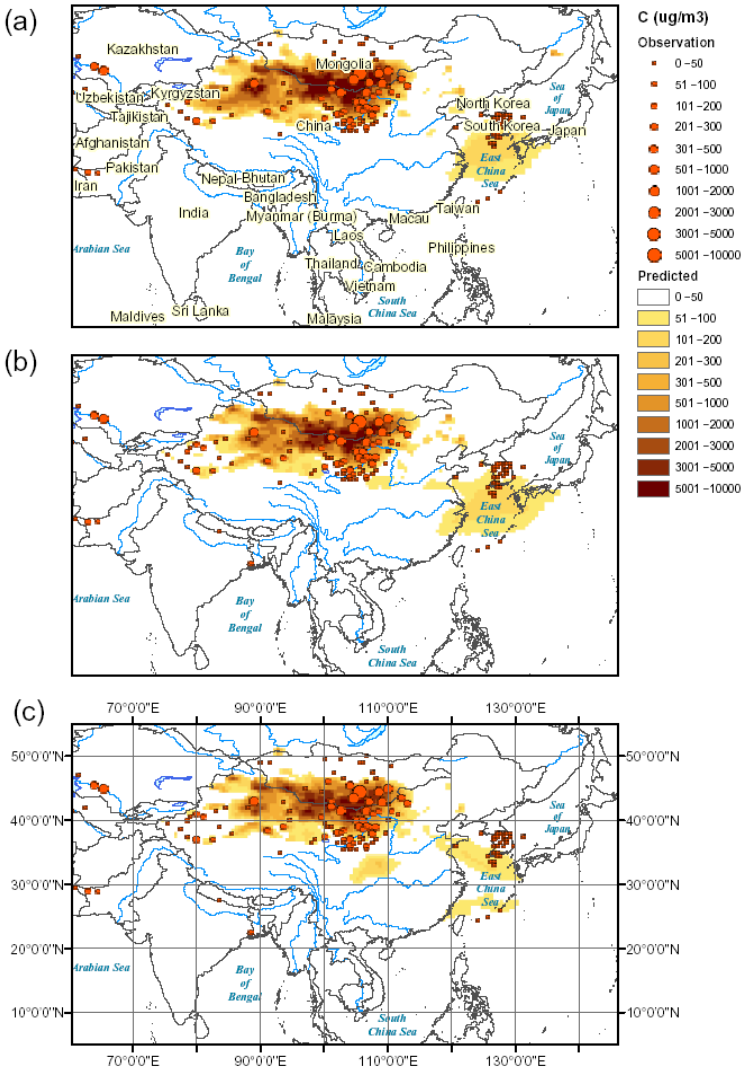

Figure 3.1: Comparisons of the predicted and observed near surface dust concentration for March 19. (a) the 24hr forecast; (b) the 48hr forecast; and (c) the 72hr forecast. Full dots represent the stations where dust activities were observed and the size of dots represents the magnitude of dust concentration.

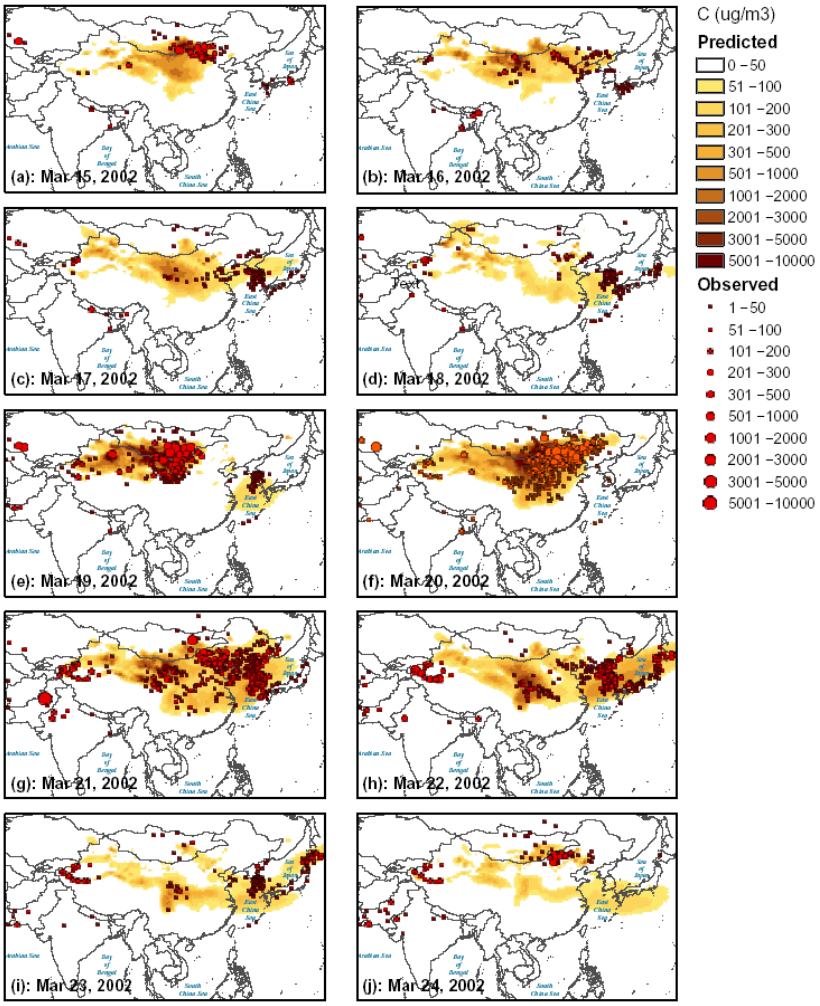

Figure 3.2: Comparisons of the predicted and observed near surface dust concentration for 10 successive days from 15 to 24 March 2002. The model results are the 24hr forecasts.

3.2 Thermodynamic phase analysis of cloud particles with FY-1C satellite data

There are many studies determining cloud particle thermodynamic phase. The underlying principle that these techniques are based on is the fact that water and ice have different absorption at 1.6μm. The ice has larger absorption at 1.6μm, so it has a lower reflectance and water has the contrary properties. Thus reflectance at 1.6μm is sensitive to the thermodynamic phase of cloud. The FY-1C polar orbiting meteorological satellite, which was launched on May 10 1999, has ten spectral channels that cover the visible, near infrared and infrared spectral bands. These data are very useful for the research of cloud particle thermodynamic phase.

According to the model calculations, one can infer that optical thickness affects the reflectance at 0.65μm greatly, the thicker optical thickness, the larger the reflectance. There is almost a linear relationship between the reflectance and optical thickness at 0.65μm. The reflectance increases monotonically at 0.65μm as a function of cloud optical thickness. The reflectance at 1.6μm is affected greatly by the effective radius of particles, the larger effective radius the smaller the reflectance. So it is known that there is a larger difference of the

reflectance between 0.65μm and 1.6μm and the reflectance at 1.6μm is smaller than that at 0.65μm when the cloud particle effective radius becomes larger. Thus ice cloud can be distinguished from water cloud by using the reflectance difference.

Case studies indicate that FY-1C multi-channel data can be efficiently used for detecting clouds and thermodynamic phase of cloud particles (Liu et al., 2002). It is helpful to improve the accuracy of geophysical parameters retrieval from meteorological satellite data. Figure 3.3 illustrates the cloud analysis results.

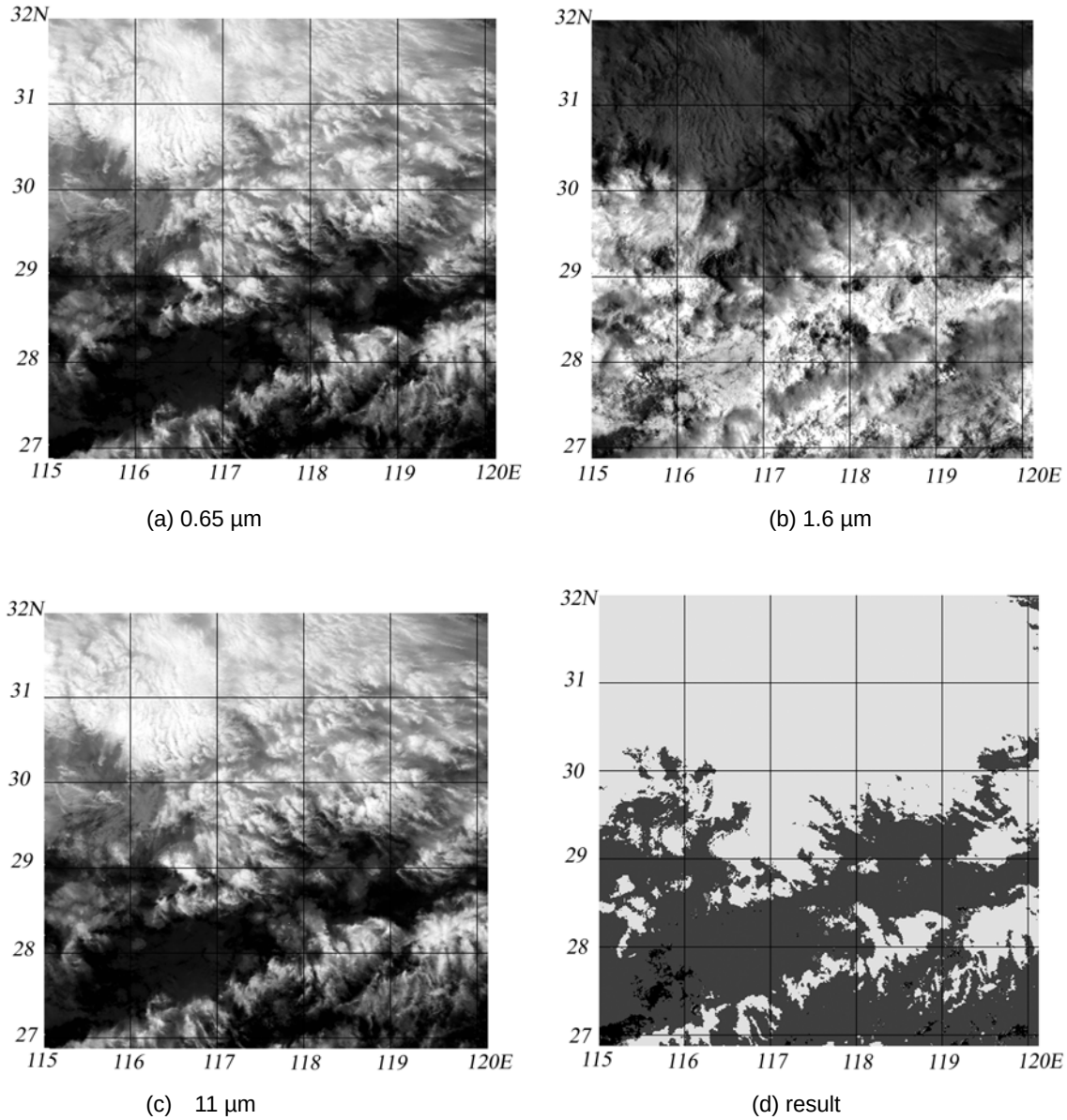

(a) 0.65 μm (b) 1.6 μm

(c) 11 μm (d) result

Figure 3.3: (a) - (c) are the 0.65 μm, 1.6 μm and 11 μm images, (d) is cloud particle thermodynamic phase results: White is ice cloud, Grey is water cloud, Black is clear

3.3 Study on 3D-VAR direct assimilation of ATOVS radiance data in NWP

Two comparison experiments, named NOAMSUA and AMSUA respectively, are carried out to simulate a very heavy rainstorm which occurred in Wuhan City and the region to the east in

July 21-22, 1998 with the incremental form of three-dimensional variational method (3D-Var) being used as the data assimilation method, and MM5 mesoscale numerical model as the assimilating and forecast model. NOAMSUA experiment assimilates radiosonde observations only, whereas AMSUA assimilates simultaneously radiosonde observations and channel brightness temperatures detected by AMSU-A which is carried on NOAA-15. The forward integration of MM5 prediction model in two comparison experiments are both conducted with assimilation analyses as model initial conditions (Pan et al., 2003).

The comparison results show that assimilating AMSU-A brightness temperature adjusts the temperature background of the middle and upper atmosphere more distinctly and the prediction of basic elements such as temperature is mostly better in the AMSU-A experiment than in the NOAMSUA experiment, which means that directly assimilating AMSU-A data has a positive impact on MM5 model prediction as a whole. It is also found in each comparison experiment that the different simulations not only influence the system of the rainstorm, southwest vortex and shear at low level but also the precipitation area. A strong precipitation phase is preferable, and the prediction of precipitation intensity almost achieves actual intensity level although prediction of 6-hours-precipitation amount is much less than actual value. Due to using AMSU-A radiances which mainly contains information of vertical air temperature distribution, assimilating AMSU-A data acts less on adjusting background of water vapor mixing ratio, which results in simulation of precipitation in AMSUA experiment not being improved too much over that in NOAMSUA experiment.

4. Summary

Meteorological satellite observations include rich information, which requires us to make great contributions to retrieval theory and algorithms. Starting from the FY-3, Chinese Meteorological satellites have a sounding capability. The FY series, with the combination of GEO/LEO satellites, will make contributions to the regional and global weather forecasting, climate and environment monitoring.

References

1. Zheng xinjiang, j. Luo, W. lu, and S. Sun, Research on Monitoring Dust Storm Using Meteorological Satellite Data, J. of Natural Disasters, 11, 210-216 (in Chinese), 2002.
2. Shao yaping, A Model for Mineral Dust Emission, J. Geophys. Res. 106, 20239-20254, 2001.
3. Shao yaping, Jung, E. J., and Leslie, L. M., Numerical Prediction of Northeast Asian Dust Storms Using an Integrated Wind Erosion Modeling System, J. Geophys. Res, 107, 4814-4824, 2002.
4. Shao, et al., Real-time Numerical Prediction of Northeast Asian Dust Storms Using an Integrated Modeling System, J. Geophys. Res (in press), 2003.
5. Liu-jian, C. Dong, and X. zhu, Thermodynamic Phase Analysis of Cloud Particles with FY-1C Data, Meteorol. Atmos. Phys. 80, 65-71, 2002.
6. Pan Ning, C. Dong, and W. Zhang, The Experiments on Direct Assimilationg ATOVS Radiance, ACTA Meteorological Sinica, 61, 226-236(in Chinese), 2003.